Crystal Structure of a Polymeric Immunoglobulin Binding Fragment of the Human Polymeric Immunoglobulin Receptor

Agnes E. Hamburger,[1,3] Anthony P. West, Jr.,[1]
and Pamela J. Bjorkman[1,2,*]
[1]Division of Biology 114-96
[2]Howard Hughes Medical Institute
California Institute of Technology
Pasadena, California 91125
[3]Division of Biology
Massachusetts Institute of Technology
Cambridge, Massachusetts 02142

Summary

The polymeric immunoglobulin receptor (pIgR) is a type I transmembrane protein that delivers dimeric IgA (dIgA) and pentameric IgM to mucosal secretions. Here, we report the 1.9 Å resolution X-ray crystal structure of the N-terminal domain of human pIgR, which binds dIgA in the absence of other pIgR domains with an equilibrium dissociation constant of 300 nM. The structure of pIgR domain 1 reveals a folding topology similar to immunoglobulin variable domains, but with differences in the counterparts of the complementarity determining regions (CDRs), including a helical turn in CDR1 and a CDR3 loop that points away from the other CDRs. The unusual CDR3 loop position prevents dimerization analogous to the pairing of antibody variable heavy and variable light domains. The pIgR domain 1 structure allows interpretation of previous mutagenesis results and structure-based comparisons between pIgR and other IgA receptors.

Introduction

Polymeric immunoglobulins (pIgs) at mucosal surfaces provide the first line of defense against pathogens and toxins. Polymeric IgA (mainly dimeric IgA; dIgA) is the predominant Ig found in secretions, with pentameric IgM (pIgM) present at lower levels (Norderhaug et al., 1999b). Unlike other antibody isotypes, IgA and IgM can form polymers via an 18-residue extension at their C termini called the tailpiece. The joining (J) chain, a 15 kDa polypeptide, promotes the oligomerization of IgA and IgM to form pIgs by crosslinking the homodimeric Fc regions of two or five antibody molecules, respectively (Halpern and Koshland, 1970; Mestecky et al., 1971). In dIgA, J-chain forms two intermolecular disulfide bonds, the first with one of two tailpieces in the first Fc homodimer and the second with a tailpiece from the second Fc homodimer. The two IgA heavy chains that are not covalently attached to J-chain form a disulfide bond to each other via Cys471 in their tailpieces (Bastian et al., 1992).

The polymeric immunoglobulin receptor (pIgR) transports pIgs across mucosal epithelia into mucosal secretions. pIgR is expressed on the basolateral surface of epithelial cells, where it binds selectively to J-chain-

*Correspondence: bjorkman@caltech.edu

containing pIgs secreted by local plasma cells (Brandtzaeg and Prydz, 1984; Radl et al., 1971; Vaerman et al., 1998a). Human pIgR binds and transports both dIgA and pIgM, whereas pIgRs from other species (e.g., rabbit, rodents, and chicken) only bind dIgA (Socken and Underdown, 1978; Underdown et al., 1992; Wieland et al., 2004). Biochemical and mutagenesis studies revealed that pIgR binding to dIgA takes place in two steps. First, the N-terminal pIgR domain (D1) makes a noncovalent interaction with the Cα3, and possibly Cα2, domains of one of the Fc regions of dIgA (Frutiger et al., 1986; Geneste et al., 1986; Hexham et al., 1999). In the second step, Cys467 in the C-terminal domain of the extracellular portion of human pIgR (D5) makes a disulfide bond with Cys311 in the Cα2 domain of the second IgA molecule (Fallgreen-Gebauer et al., 1993). pIgR/pIg complexes are transcytosed to the apical surface of the epithelial monolayer, where the pIgR/pIg complex is released from the membrane by the proteolytic cleavage of pIgR, forming secretory Ig (SIg). The cleaved ectodomain of human pIgR, also known as secretory component (SC), is covalently attached via a disulfide bond to dIgA or noncovalently to pIgM (Brandtzaeg, 1975; Mostov et al., 1980). Free SC that is not complexed to a pIg is also released into secretions (Brandtzaeg, 1973).

pIgR is a glycosylated type I transmembrane protein, consisting of a 620 residue extracellular region, a 23 residue transmembrane region, and a 103 residue cytoplasmic tail. The extracellular region contains five domains (domains 1–5; D1–D5) that share sequence similarity with Ig variable (V) regions (Mostov et al., 1984). Thus, the pIgR D1-D5 domains are predicted to be β sandwich structures each containing two β sheets (composed of strands A, B, E, and D and strands C″, C′, C, F, G, and A′ in the case of D1–D4, and strands A, B, E, D and strands A′, C, F, and G in the case of D5). D1–D4 each contain regions homologous to the three antigen binding complementarity-determining region (CDR) loops of Ig variable domains.

Mutagenesis and peptide binding studies have identified probable binding sites on pIgR and dIgA. pIgR D1 is necessary and sufficient for binding to dIgA (Frutiger et al., 1986) and all three of its CDR loops have been implicated in the interaction with the antibody (Coyne et al., 1994). Potential pIgR binding sites on dIgA involve the dIgA Cα3 domain and include residues 402–410 in the loop connecting strands D and E and residues 430–443 in the FG loop (Hexham et al., 1999; White and Capra, 2002). Since pIgR preferentially binds and transcytoses dIgA molecules containing J-chain, pIgR D1 may also directly interact with J-chain (Brandtzaeg and Prydz, 1984; Vaerman et al., 1998a, 1998b). In order to contribute to the molecular description of the interaction between pIgR and pIgs, we determined the 1.9 Å crystal structure of a pIg binding fragment of the human pIgR consisting of the N-terminal or D1 domain. The structure reveals an Ig variable-like domain that allows interpretation of previous mutagenesis studies and comparison with other IgA receptors.
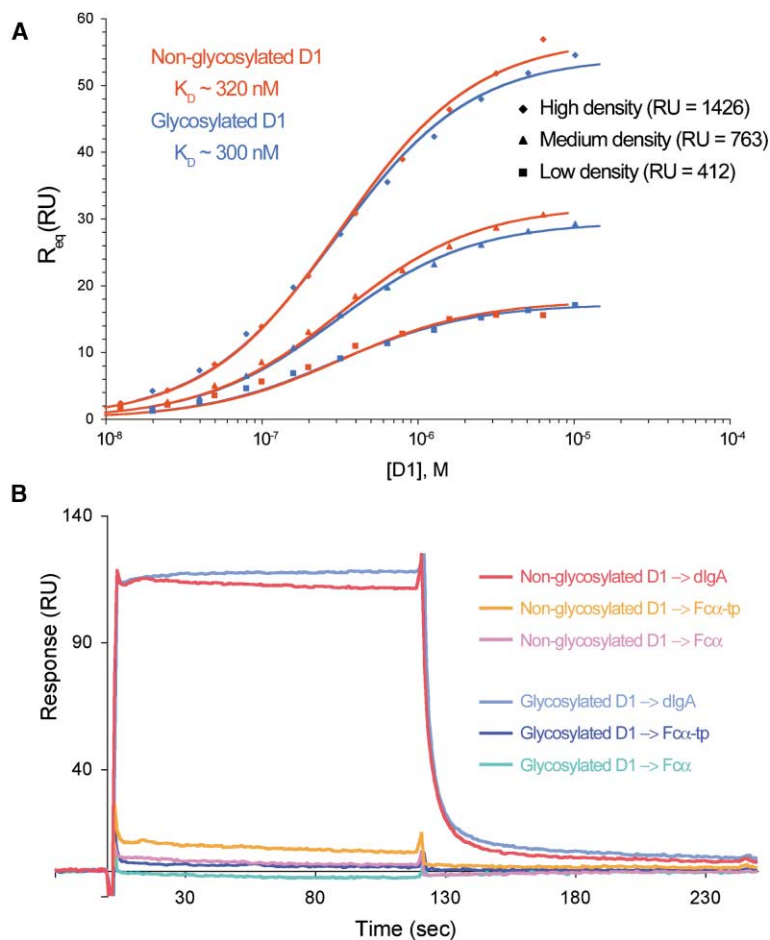
Figure 1. Biosensor Analyses of pIgR D1 Binding to dIgA

(A) Equilibrium binding data for biosensor experiments in which nonglycosylated (expressed in bacteria) and glycosylated (expressed in insect cells) versions of pIgR D1 were injected over dIgA immobilized at three different densities (412, 763, and 1426 RUs). The plot shows the equilibrium binding response (R_{eq}) versus the log of concentration of the indicated proteins. Best-fit binding curves based on a 1:1 binding model are superimposed on the binding data.

(B) Sensorgram from binding experiments in which 5 μM glycosylated or nonglycosylated forms of D1 were injected over monomeric (with and without the tailpiece) and dimeric versions of the IgA Fc region. The injected protein is indicated in front of an arrow pointing to the immobilized protein.

Results and Discussion

Biosensor Binding Experiments

The ligand binding domain of human pIgR, an Fc receptor that is specific for dimeric and polymeric forms of IgA and IgM, was expressed in *E. coli* and refolded from inclusion bodies. A glycosylated form of the protein was also expressed in baculovirus-infected insect cells. D1 was tested for binding to dimeric and monomeric versions of the IgA Fc region. For the dimeric version of IgA, we used dIgA/J-chain complexes purified from human serum (Vaerman et al., 1995), and for the monomeric version, we used recombinant IgA Fc regions expressed in CHO cells. One Fc region was expressed without the tailpiece (Fcα) as described (Herr et al., 2003b), and the other Fc region included the tailpiece (Fcα-tp). Binding was evaluated using a surface plasmon resonance-based binding assay. Both the glycosylated and nonglycosylated forms of D1 bind to dIgA with an equilibrium dissociation constant (K_D) of ∼300 nM (Figure 1A), consistent with other binding studies (Bakos et al., 1994). Both versions of D1 show greatly reduced or negligible binding to the monomeric Fcα and Fcα-tp proteins at concentrations up to 5 μM (Figure 1B). By contrast, another IgA Fc receptor, FcαRI, binds dIgA, Fcα-tp, and Fcα when injected at a concentration of 5 μM (data not shown) (Herr et al., 2003b).

Structure of pIgR D1

The 1.9 Å crystal structure of the human pIgR D1 was solved by multiple isomorphous replacement with anomalous scattering (MIRAS). As predicted by sequence analysis, the folding topology of pIgR D1 resembles the topologies of Ig variable heavy (V_H) and variable light (V_L) domains (Mostov et al., 1984). Like Ig variable domains, pIgR D1 contains ten β strands assembled into two antiparallel β sheets with strands A, B, E, and D on one face and C″, C′, C, F, G, and A′ on the other (Figures 2A–2C). Five residues that are characteristic of Ig regions (Williams and Barclay, 1988) are found in the expected positions in pIgR D1: Cys22 and Cys92, which form a disulfide bond linking the two β sheets, Trp37, the "invariant" tryptophan (Figure 2D) that packs into the hydrophobic core, and Arg63 and Asp86, which form a salt bridge (Figure 3). In addition, pIgR D1 contains a second disulfide bond between Cys38 and Cys46 that link the C and C′ strands, which is also found in NKp44, a natural killer cell cytotoxicity activating receptor (Cantoni et al., 2003).

Antibody V_H and V_L domains each contain three hypervariable complementarity-determining region (CDR) loops (CDR1, CDR2, and CDR3), which together form the antigen combining site in a V_H-V_L heterodimer (Alzari et al., 1988). Although the pIgR D1 structure closely resembles an isolated Ig variable domain, the positions
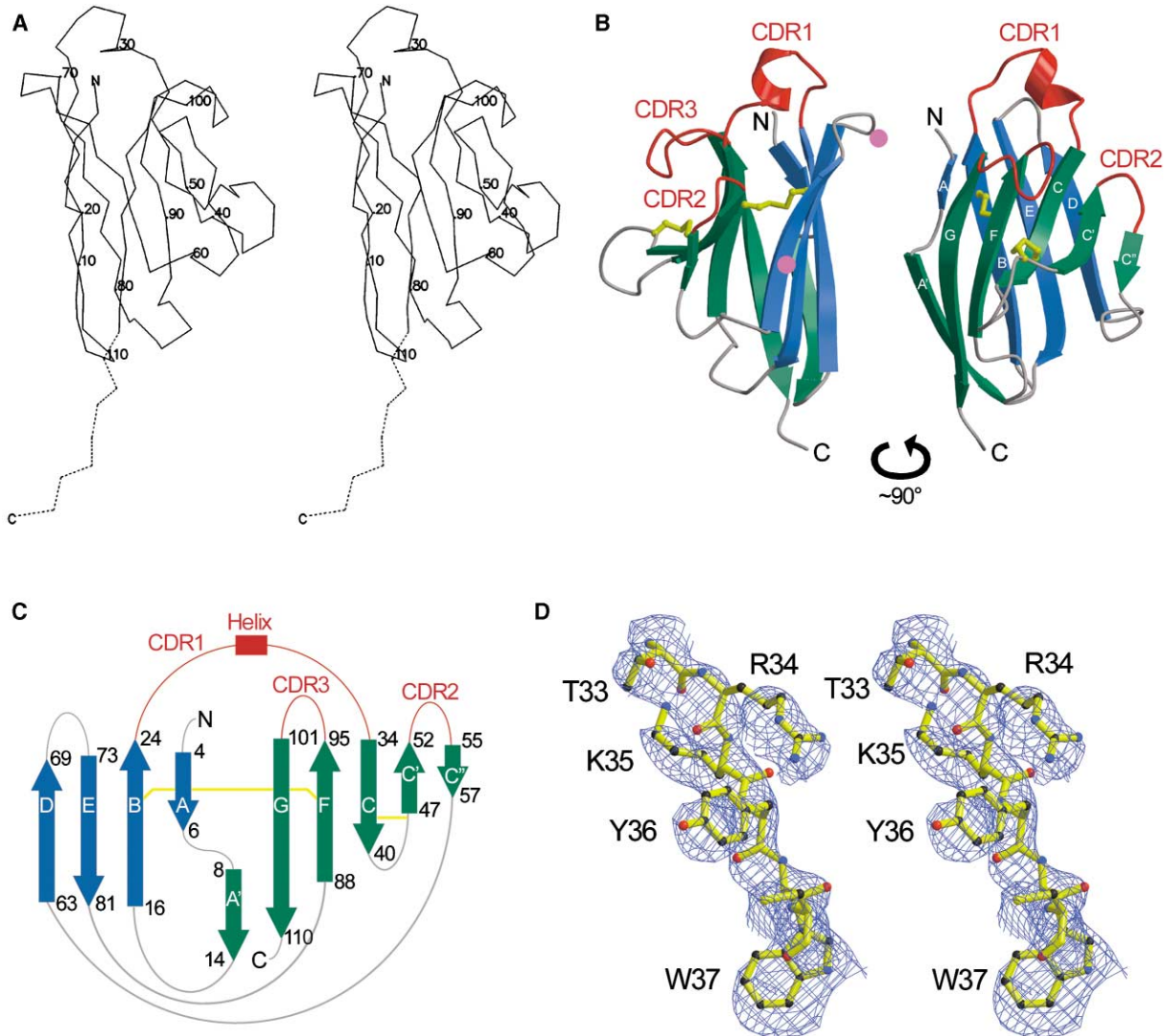
Figure 2. The Structure of Human pIgR D1

(A) Cα trace (molecule E). The 6×His tag from molecule A (dashed line) was superimposed onto molecule E.

(B) Ribbon diagram showing side and front views of pIgR D1. β strands A, B, E, and D are shown in blue, β strands C″, C′, C, F, G, and A′ are in green, and the three CDR loops (including the α helix within CDR1) are red. Cysteines involved in disulfide bonds are shown in yellow in ball-and-stick representation and the locations of potential N-linked glycosylation sites are indicated by pink spheres.

(C) Topology diagram of pIgR D1. The color schemes for the β strands, α helix, and CDR loops are the same as in (A).

(D) Stereoview of the pIgR D1 model in the region of the "invariant" tryptophan, Trp37, superimposed on a 2.7 Å experimental electron density map (calculated with MIRAS phases) contoured at 1.0 σ.

of the three CDR loops in D1 differ substantially from their antibody counterparts. Comparative analyses of the CDR regions in antibody structures have allowed classification of CDR loops into a set of canonical structures (Chothia and Lesk, 1987). Although the sequence of the D1 CDR1 loop shares similarity with sequences found in type 1 of the six canonical CDR1 structures in Ig Vκ domains (Bakos et al., 1993), the CDR1 structure in pIgR D1 differs considerably. Unlike any of the canonical structures for CDR1 loops in V_L or V_H domains (Al-Lazikani et al., 1997), the pIgR D1 CDR1 includes a single helical turn composed of residues that are highly conserved among sequences of pIgR from different species (Figure 3). By contrast, CDR1 loops in V_H and V_L domains

are composed of extended structures joined by short links or hairpin turns (Chothia et al., 1989). CDR2 and CDR3 in pIgR D1 do not appear to resemble any of the canonical sequence or structure patterns. The pIgR CDR2 loop is very short, with only two residues in the loop region between the C′ and C″ strands. By contrast, CDR2 loops in Vκ domains consist of three residues that form a classic γ turn (Al-Lazikani et al., 1997). Unlike its position in antibody V_H and V_L domains, the CDR3 loop of pIgR D1 is tilted toward the C″C′CFGA′ sheet, away from the other CDRs (Figure 4A). A conserved hydrophobic residue, Tyr36, is buried at the interface of the D1 CDR3 and the C″C′CFGA′ sheet (Figure 4B). The position of the CDR3 loop is stabilized by hydrogen
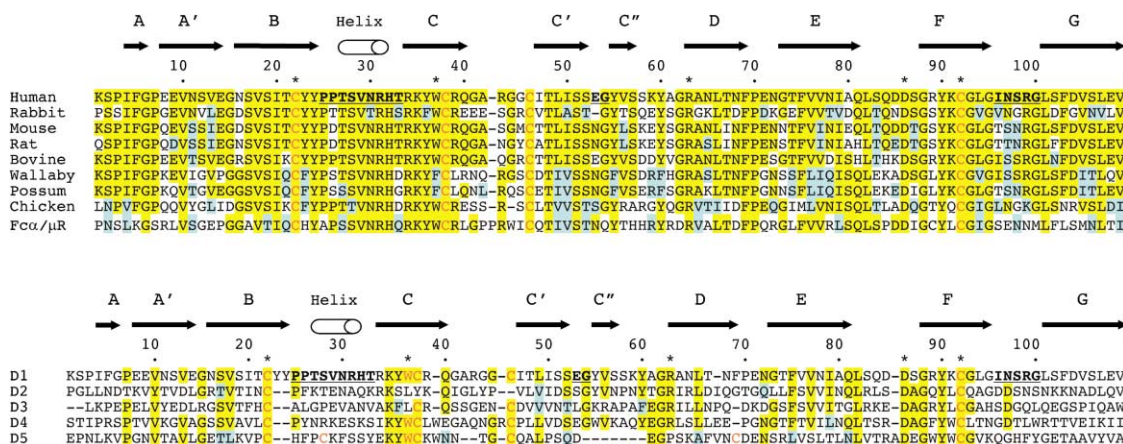
Figure 3. Amino Acid Sequence Alignment of Human pIgR D1 and Related Proteins

Top: pIgR D1 from eight different species and the Ig-like domain from the human Fcα/μR were aligned. Cysteines involved in disulfide bonds are shown in red, conserved residues are highlighted in yellow, and conservatively substituted residues are highlighted in blue. Asterisks indicate the positions of five characteristic residues in Ig V domains. Sequences within the three CDR loops are shown in bold and underlined. Crystallographically determined secondary structure elements are shown above the sequences. Accession codes for the pIgR sequences are: P01833 (human), P01832 (rabbit), O70570 (mouse), P15083 (rat), P81265 (bovine), AAK69593 (*Macropus eugenii* [tammar wallaby]), AAD41688 (*Trichosurus vulpecula* [silver-gray brushtail possum]), and AAP69598 (*Gallus gallus* [chicken]), and AAL51154 (human Fcα/μR). Bottom: the D1 domain of pIgR is aligned with the other domains within the human pIgR extracellular region.

bonds between Asn97 within the loop and two residues on the C″C′CFGA′ sheet: Arg34 in the C strand and Thr48 in the C′ strand. The observed conformation of the D1 CDR3 loop is likely to represent its conformation in solution because the loop is not involved in crystal contacts. The different orientation of the pIgR CDR3 loop as compared to the CDR3 loops of Ig V domains (Figure 4A) is consistent with why D1 does not form dimers analogous to antibody V_H-V_L heterodimers (Figure 4C) or V_L-V_L homodimers. When pIgR D1 is superimposed on an Ig V_H-V_L combining site (Zdanov et al., 1994) (Figure 4C) to create a D1 dimer, the CDR3 regions clash with the CC′ loop from the partner molecule (Figure 4D). Although two different dimers of pIgR D1 are observed in the crystal packing, neither is analogous to Ig V_H-V_L dimers. The D1 dimers in the crystals are unlikely to be biologically relevant because there are two different dimeric arrangements and the D1 protein migrates in the position expected for a monomer on a gel filtration column (data not shown).

Although the protein used for our structural studies is not glycosylated because it was expressed in bacteria, the pIgR D1 structure can be used to locate residues to which carbohydrate would normally be attached. Human pIgR D1 contains two N-linked carbohydrates attached to Asn65 and Asn72 (Hughes et al., 1999). These residues are located on the D strand and the DE loop, respectively, and their sidechains are accessible to solvent (Figure 2B). Studies comparing the binding of bacterially expressed nonglycosylated D1 with glycosylated D1 expressed in insect cells revealed nearly identical binding affinities for dIgA (Figure 1A), consistent with earlier studies showing that pIgR glycosylation is not necessary for specific binding to dIgA (Bakos et al., 1991). Carbohydrates may be required, however, for efficient transport or release of the pIgR ectodomain during transcytosis of dIgA, since nonglycosylated pIgR

is released from the apical surface at low levels (Matsumoto et al., 2003). In addition, carbohydrates on SC contribute to stabilization of SIgs by protecting it from proteolytic degradation (Crottet and Corthesy, 1998).

Structure-Based Interpretations of Binding Studies

Previous mutational and peptide-mapping experiments to define the regions of pIgR that form the binding sites for dIgA and pIgM can now be interpreted using the pIgR D1 structure. CDR1 of pIgR D1 was proposed to make essential contacts with dIgA because it is the most highly conserved region of D1 among different species of pIgR, and a synthetic peptide corresponding to residues 15–37 of SC, a region that contains the D1 CDR1 loop, is capable of binding pIgs (Bakos et al., 1991). Interestingly, this peptide binds Igs indiscriminately, interacting with pIgs as well as with monomeric IgA and IgG (Bakos et al., 1991). The promiscuous binding of this peptide suggests that other parts of D1, in addition to the CDR1 loop, likely contribute to pIg binding specificity. The D1 structure reveals a solvent-exposed helix within the CDR1 loop containing residues with the potential to make direct contacts with pIgs (Figure 5).

Point mutations in the CDR1 region of the rabbit pIgR D1 highlighted the importance of three charged residues (two arginines and a lysine, which correspond to Arg31, Arg34, and Lys35 in the sequence of human pIgR D1). Substitution of these residues with alanine abolished pIgR binding to dIgA (Coyne et al., 1994). The human pIgR D1 structure shows that Arg31 (rabbit Arg37) is solvent exposed and could interact directly with dIgA. Although Arg34 and Lys35 were predicted to be in the CDR1 loop (Coyne et al., 1994), an analysis of main chain hydrogen bonds in the D1 structure shows that they are both in the C strand. Arg34 is the first residue in the strand, as its main chain carbonyl group forms a hydro-
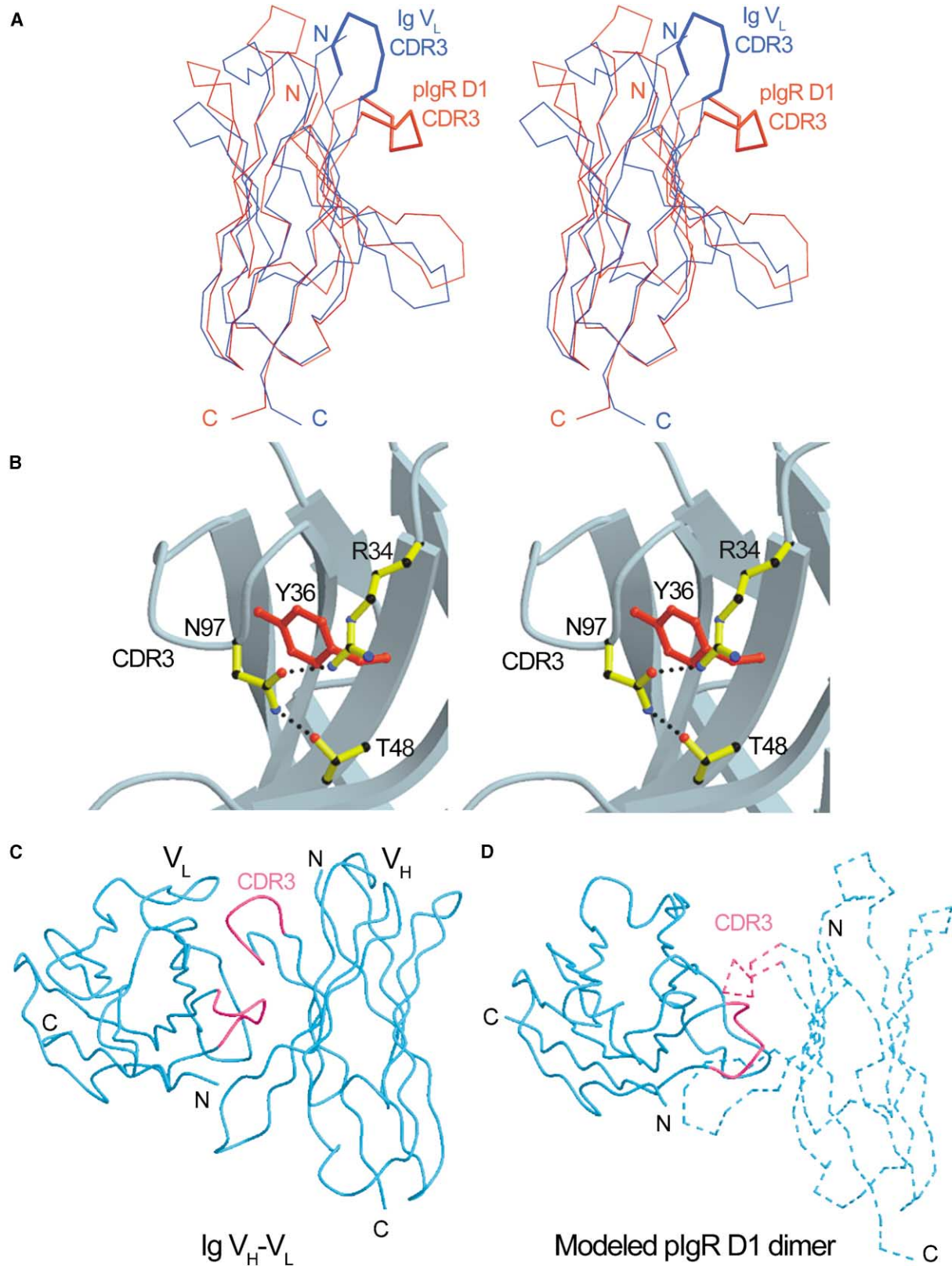
Figure 4. Structural Consequences of the Position of the pIgR D1 CDR3 Loop

(A) Stereoview of the superposition of pIgR D1 (red) with an Ig V_L domain (blue) derived from a mouse single-chain Fv (PDB code 1MFA).
(B) Stereoview of the region in the vicinity of the pIgR D1 CDR3 loop showing Tyr36 buried at the interface between CDR3 and the C″C′CFGA′ sheet. A ball-and-stick representation of Tyr36 is shown in red. Atoms in residues that stabilize this position of CDR3 are highlighted with an atom-based color code (carbon, black; oxygen, red; nitrogen, blue), and hydrogen bonds are indicated as black dashed lines.
(C and D) Comparison of an Ig V_H-V_L heterodimer (PDB code 1MFA) (C) with a computer model of a pIgR D1 homodimer (D) created by superimposing D1 on the V_H and V_L domains of a V_H-V_L heterodimer (C). The rmsd values are 1.39 Å for the V_H-D1 superposition (calculated for 101 Cα atoms) and 1.38 Å for the V_L-D1 superposition (calculated for 78 Cα atoms). CDR3 loops are highlighted in pink.
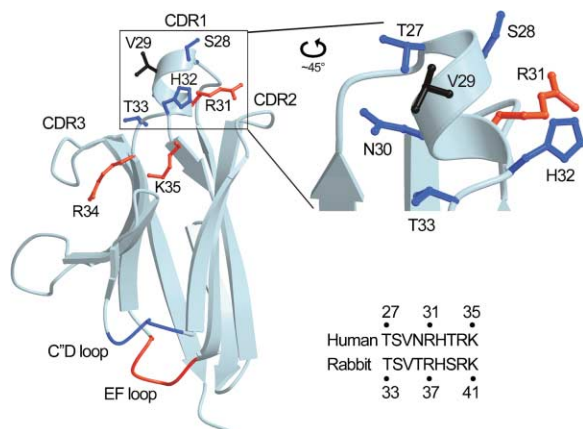
Figure 5. Mutagenesis Data Mapped onto Structure

The positions of substitutions that abolished (red) or decreased (blue) pIgA binding to rabbit pIgR (Coyne et al., 1994) are mapped onto the human pIgR D1 structure. A close-up of the CDR1 region is shown in the upper right, and the sequence of CDR1 in human and rabbit pIgR D1 is shown in the lower right. Val29 (black), which is solvent exposed in the D1 structure, was assumed to be buried and was therefore not substituted (Bakos et al., 1993; Coyne et al., 1994).

gen bond with the main chain amino group of Gly95 in the F strand. Human D1 Arg34 (rabbit Arg40) points in the opposite direction from Arg31 and is occluded by the CDR3 loop, forming a hydrogen bond to CDR3 loop residue Asn97 (Figure 4B). Arg34 is thus unlikely to interact directly with a ligand, but may affect ligand binding indirectly by stabilizing the CDR3 loop. This interpretation is consistent with the results of mutagenesis experiments involving rabbit pIgR in which replacing the rabbit counterpart of Arg34 with a glutamic acid, a residue that can still form a hydrogen bond with Asn97 in CDR3, had no affect on ligand binding, whereas substitution to an alanine, which cannot form the hydrogen bond, abolished binding (Coyne et al., 1994). Lys35 (rabbit Lys41) is buried between the two β sheets and is also unlikely to represent a direct point of contact with the antibody. However, it stabilizes the position of the CDR1 loop by forming hydrogen bonds with Arg31 and Thr33 in the conserved helical turn in the CDR1 loop (Figure 5). Single point mutations in surrounding residues corresponding to human pIgR residues Thr27, Ser28, Asn30, His32, and Thr33 resulted in decreased dIgA binding (Coyne et al., 1994). Residues Ser28 through His32 comprise the helical turn in CDR1 and, together with the adjacent Thr27 and Thr33, are surface exposed in positions that could interact with dIgA directly. The rabbit counterpart of human D1 Val29 was not substituted because it was predicted to be buried (Bakos et al., 1993; Coyne et al., 1994), however, the crystal structure reveals that it is a surface-exposed residue located on the helix within the CDR1 loop (Figure 5). Although its role in binding dIgA is difficult to predict because it points in the opposite direction from another critical residue, Arg31, solvent-exposed hydrophobic residues are often located at binding interfaces (Dall'Acqua et al., 1996; Kelley and O'Connell, 1993; Lebron and Bjorkman, 1999; Tsumoto et al., 1995; Vaughn et al., 1997; Wells and de Vos, 1996).

In addition to CDR1, mutagenesis and binding experiments using rabbit pIgR have implicated the other CDRs in binding dIgA. Replacing the CDR2 or CDR3 regions in D1 with their corresponding regions from D2 results in complete loss of dIgA binding (Coyne et al., 1994). The human pIgR D1 structure reveals that CDR3 is positioned away from the other CDRs (Figure 2B), unlike the CDR3 loops of Ig V domains, which form a contiguous binding surface with CDRs 1 and 2 (Alzari et al., 1988). It may therefore be difficult for a ligand contacting the CDR1 and CDR2 regions of pIgR D1 to simultaneously contact CDR3. Thus it is possible that the loss of affinity upon replacing the D1 CDR3 with another sequence may be due to steric interference with dIgA binding rather than alteration of a direct binding surface. The results of other loop replacements are harder to interpret using the pIgR D1 structure: replacing the rabbit D1 EF loop with its counterpart in D2 led to the loss of dIgA binding, whereas replacing the C″D loop had little effect (Coyne et al., 1994). Both loops are on the opposite side of the D1 domain from the CDRs (Figure 5), and are not expected to contact the ligand.

Although human pIgR binds both dIgA and pIgM, rabbit pIgR only binds dIgA (Roe et al., 1999; Socken and Underdown, 1978). By taking advantage of these binding differences, studies using site-directed mutants and human/rabbit chimeric pIgR molecules have identified regions required for binding pIgM (Roe et al., 1999). All three CDR loops were shown to contribute to binding pIgM, but to different extents. For maximal binding of rabbit pIgR to pIgM, replacing all three CDR loops with their human counterparts was required, but CDR2 appears to be the most critical: replacing rabbit CDR2 with the human equivalent transferred pIgM binding, and replacing human CDR2 with the rabbit sequence resulted in substantial loss of binding (Roe et al., 1999). Sequence alignment shows large differences in the human and rabbit CDR2 loops, including a deletion of a charged residue, Glu54, in the rabbit CDR2 (Figure 3). Thus, deletion of the surface-exposed Glu54 may eliminate a point of electrostatic interaction between pIgR and pIgM. Interestingly, only bovine and human pIgR D1 regions contain the glutamic acid in their CDR2 loops (Figure 3), and these are the only species of pIgR that show high affinity pIgM binding (Socken and Underdown, 1978).

The Human pIgR D1 Structure as a Model for Similar Domains

Amino acid sequence alignment of pIgR D1 sequences from eight different species reveals conservation of residues identified as critical for the human pIgR D1 structure (Figure 3), thus the human pIgR D1 structure can be used as a first-order model for the D1 domains of pIgR proteins from other species. In addition to the five residues characteristic of Ig V domains (asterisks in Figure 3), the cysteines that participate in the second disulfide bond and the three CDR loops (which are 67%–100% conserved in CDR1, 50%–100% in CDR2, and 40%–80% in CDR3), residues that participate in anchoring the CDR1 and CDR3 loops are also highly conserved. All of the residues comprising the helical turn in CDR1

are either conserved or conservatively substituted in all eight species, and Lys35, a buried residue that stabilizes the helix, is also conserved (Figure 3). Tyr36, the residue buried under the CDR3 loop (Figure 4B), is conserved in 7 of 8 species of pIgR, and conservatively substituted by a phenylalanine in the eighth species (rabbit) (Figure 3). Three other residues that interact to stabilize the CDR3 loop position are either conserved or conservatively substituted in D1 sequences: CDR3 residue Asn97 (a polar residue in all sequences), Arg34 (conserved), and Thr48 (conserved) (Figure 3). Conservation of these critical residues suggests that the helical turn in CDR1 and the unusual CDR3 location observed in the human pIgR D1 structure are preserved in other pIgR D1 domains. The most notable difference in the D1 sequence alignments is seen in the CC′ loop in all of the sequences.

The pIgR D1 structure can also be used to make predictions about the structures of the remaining domains in the human pIgR extracellular region. The characteristic disulfide bond seen in members of the Ig superfamily (Williams and Barclay, 1988) is retained in all five domains. Also, pIgR domains 3, 4, and 5 each contain cysteines in positions to make the second disulfide bond that bridges the C and C′ β strands of D1 (Figure 2C). In addition, D5 contains a third disulfide bond that rearranges as a result of the covalent association with dIgA, whereby Cys467 of pIgR is linked to Cys311 in the IgA heavy chain (Fallgreen-Gebauer et al., 1993). The characteristic salt-bridge in Ig-like domains, which involves Arg63 and Asp86 in D1, is conserved in D2–D4, and the "invariant" tryptophan is present in D4 and D5 (Figure 3). By contrast with these conserved sequence features, which suggest an overall similar folding topology to that observed for the human D1 structure, the three CDR loops in human pIgR D1 do not share significant sequence identity with their counterparts in D2–D5 (Figure 3), suggesting local differences in loop structures. Such differences are not unexpected since the CDR loops are implicated in binding to dIgA, and only D1 can bind to dIgA in isolation (Frutiger et al., 1986). Overall, the sequences of D2–D5 are more variable than D1 across species (Piskurich et al., 1995). This observation is not surprising given the differences across species that D2–D5 make to dIgA binding. In the case of human pIgR, D2 and D3 enhance pIgR's affinity for dIgA (Norderhaug et al., 1999a). The presence of D2–D3 in bovine pIgR also increases ligand binding affinity (Beale, 1988), but D2–D5 in rabbit pIgR do not contribute significantly to dIgA binding (Frutiger et al., 1986). Thus, the full-length ectodomain (D1–D5), an alternatively spliced version (lacking D2–D3), and D1 of rabbit pIgR bind to pIgs with similar affinities (Deitcher and Mostov, 1986; Frutiger et al., 1986). Murine pIgR D2–D3 are not necessary for high affinity noncovalent binding to dIgA (Crottet and Corthesy, 1999), and chicken pIgR contains only four extracellular Ig-like domains, with no ortholog to D2 of mammalian pIgRs (Wieland et al., 2004).

Sequence alignment suggests that human pIgR D1 also shares structural similarities with the corresponding region of another IgA and IgM receptor, the Fcα/μ receptor (Fcα/μR) (Figure 3) (Shibuya et al., 2000). Fcα/μR, which can bind to monomeric and polymeric IgA and

IgM, but not IgG, is expressed by the majority of B lymphocytes and macrophages (McDonald et al., 2002; Shibuya et al., 2000). Human pIgR D1 and the Ig-like domain of Fcα/μR share 43% sequence identity. The five characteristic residues in Ig V domains (Figure 3) and the second disulfide bond linking strands C and C′ are conserved between pIgR D1 and Fcα/μR, suggesting similar tertiary structures. In addition, Fcα/μR shares 67% sequence identity with pIgR D1 in one of the identified ligand binding sites, the CDR1 loop, including complete conservation of all of the residues that comprise the helical turn within this loop in pIgR D1. The unusual CDR3 position is potentially another feature shared by the two proteins since the buried D1 residues Tyr36, Arg34, and Thr48 are conserved in Fcα/μR, and D1 Asn97 is replaced by a glutamic acid. A hydrogen bond between Fcα/μR Glu97 and Thr48 (analogous to the Asn97 to Thr48 hydrogen bond in pIgR D1) and a salt bridge between Fcα/μR Glu97 and Arg34 (replacing the hydrogen bond in pIgR D1 between Asn97 and Arg34) (Figure 4B) would preserve the downward orientation of the CDR3 loop. The overall conservation of structurally important residues within the CDR loops of Fcα/μR and pIgR D1 suggests a similar mode of interaction with the common ligands of these receptors.

Another IgA receptor, FcαRI, shares an overlapping binding site on the IgA Fc region with pIgR that includes the FG loop of Fcα (Herr et al., 2003a; Hexham et al., 1999; White and Capra, 2002). The overlap of the binding site has been suggested (Herr et al., 2003a) to explain why secretory IgA (dIgA plus the pIgR ectodomain) cannot bind to or activate FcαRI in the absence of an integrin coreceptor (van Egmond et al., 2000; Vidarsson et al., 2001). Although pIgR and FcαRI appear to recognize at least some of the same portion of Fcα, their structures do not share detailed common features beyond the fact that both molecules are Ig superfamily members. The crystal structure of an FcαRI/Fcα complex shows that the site on FcαRI at the interface with Fcα involves residues in the FcαRI BC loop, the D strand, the DE loop, and the FG loop (Herr et al., 2003a). The BC and FG loops in FcαRI are topologically equivalent to CDR1 and CDR3, respectively, but are not technically CDRs because FcαRI does not resemble an Ig variable domain. Further, the two Ig-like domains of FcαRI lack C″ strands and therefore a loop equivalent to the CDR2 region. Thus, although pIgR and FcαRI bind to the same or to an overlapping site on Fcα, they do so with different recognition modes and folding topologies. Further structural studies of pIgR in complex with dimeric Fcα will be required to compare the recognition properties of pIgR, Fcα/μR, and FcαRI, and to fully understand the mechanism by which pIgR is specific for the binding and transport of polymeric Igs.

Experimental Procedures

Protein Expression and Purification

The cDNA encoding the full-length human pIgR was kindly provided by Roland Strong (Fred Hutchinson Cancer Research Center, Seattle, WA). For bacterial expression, pIgR D1 (encoding residues Lys1–Val109) was subcloned into the pET20b expression vector (Novagen) in frame with the C-terminal 6×His tag using the following primers: 5′-G GAA TCC CAT ATG AAG AGT CCC ATA TTT GGT CC-3′ and

Table 1. Data Collection, Phasing, and Refinement Statistics for pIgR D1

Data Set	Wavelength (Å)	Resolution (Å)	No. Unique Reflections/Total Reflections	Completeness (%)[a]	Twin Fraction (%)	R_{merge} (%)[b]	I/σ	Phasing Power[c]
Native I	1.54	2.5 (2.59–2.50)	21,524/76,172	97.4 (80.7)	26.5	8.5 (34.3)	19.6 (2.5)	
Native II	1.078	1.9 (1.93–1.90)	49,755/185,798	99.6 (99.1)	37.3	7.8 (46.2)	17.7 (2.6)	
PIP	1.54	3.2 (3.31–3.20)	10,464/28,678	98.5 (94.3)	20.7	9.7 (20.8)	11.3 (5.3)	0.4
Gd	1.7108	2.8 (2.85–2.80)	27,967/47,501	89.6 (58.7)	30.3	10.4 (41.3)	8.6 (1.5)	1.0
Pb	0.9509	2.0 (2.03–2.00)	79,649/153,910	94.1 (92.7)	37.0	6.5 (23.8)	12.2 (3.5)	0.6

Refinement Statistics (P2₁)		Number of Nonhydrogen Atoms	
Resolution (Å)	30–1.9	Protein	4993
Number of reflections in working set	47,117 (93.4%)	Water	158
Number of reflections in test set	2,476 (4.9%)	Mg^{2+}	2
R_{cryst} (%)[d]	18.3		
R_{free} (%)[e]	24.4		

		Ramachandran plot quality (%)	
		Nonglycine residues in	
		most favored	87.3
Rmsd from ideality		additionally allowed	12.3
Bond lengths (Å)	0.007	generously allowed	0.4
Bond angles (deg)	1.30	disallowed	0.0

Values in parentheses indicate data in the highest resolution shell.

[a] Completeness is defined as the number of independent reflections/total theoretical number.

[b] $R_{merge} = 100 \times \Sigma(|I - <I>|)/\Sigma I$, where I is the integrated intensity of a given reflection.

[c] Rms f_h/E (phasing power), where f_h is the heavy atom structure factor amplitude and E is the lack of closure error. The phasing power statistics were derived using twinned data and may therefore not be accurate.

[d] $R_{cryst}(F) = \Sigma_h||F_{obs}(h)| - |F_{calc}(h)||/\Sigma_h|F_{obs}(h)|$, where $|F_{obs}(h)|$ and $|F_{calc}(h)|$ are the observed and calculated structure factor amplitudes for the hkl reflection.

[e] R_{free} is calculated from reflections in a test set not included in the atomic refinement.

5′-GG AAT TCA CTC GAG GAC CTC CAG GCT GAC-3′. The protein was expressed in *E. coli* BL21(DE3) cells (Novagen) by induction at OD_{600} = 0.5 − 0.6 with isopropyl-β-D-thiogalactoside (IPTG) at a final concentration of 0.4 mM for 5 hr at 37°C. pIgR D1 inclusion bodies were solubilized in 8 M guanidine-HCl and 10 mM DTT. The protein was refolded by the rapid dilution method in refolding buffer (100 mM Tris [pH 8.0], 400 mM L-arginine, 2 mM EDTA, 0.5 mM oxidized glutathione, and 5 mM reduced glutathione) (Garboczi et al., 1992). The refolded protein was concentrated in a stirred-cell pressurized concentrator (Amicon) and loaded onto a Superdex 75 26/60 column (Amersham Biosciences) for size exclusion chromatography.

For insect cell expression to produce glycosylated protein, pIgR D1 containing a C-terminal 6×His tag was subcloned into the baculovirus transfer vector pAcGP67A (BD Biosciences) in frame with the gp67 secretion signal. Recombinant baculovirus was generated by cotransfection of the transfer vector with linearized viral DNA (Baculogold; BD Biosciences). pIgR D1 was harvested from the supernatant of baculovirus infected High 5 insect cells, which was concentrated and buffer exchanged into TBS (20 mM Tris [pH 8.0], 150 mM NaCl) and purified by Ni-NTA affinity followed by size exclusion chromatography on a Superdex 200 16/60 column (Amersham Biosciences).

Human pIgA isolated from the sera of a patient with a pIgA-producing myeloma was kindly provided by Jean-Pierre Vaerman (Catholic University of Louvain, Brussels, Belgium) (Song et al., 1995; Vaerman et al., 1995). pIgA was further purified by size exclusion chromatography on a Superdex 200 HR 10/30 column (Amersham Biosciences) to separate dIgA from higher order polymers. The peak corresponding to dIgA (two IgA molecules linked by J-chain) was used for the binding studies. Soluble FcαRI and monomeric Fcα (Fcα homodimers lacking a tailpiece that are not linked by J-chain) was purified from the supernatants of stably transfected Chinese hamster ovary (CHO) cells as described previously (Herr et al., 2003b). Monomeric Fcα with the 18 residue tailpiece (Fcα-tp) and an N-terminal 6×His tag was generated and purified as described for Fcα (Herr et al., 2003b).

Protein concentrations were determined spectrophotometrically at 280 nm using extinction coefficients of 13,370 $M^{-1}cm^{-1}$ for pIgR D1 and 64,940 $M^{-1}cm^{-1}$ for monomeric Fcα and Fcα-tp, calculated from their amino acid sequences using the ProtParam tool on the ExPASy Proteomics Server (Gill and von Hippel, 1989).

Binding Studies

Surface plasmon resonance (SPR) biosensor assays were carried out using a BIAcore 2000 instrument (Pharmacia Biosensor, Uppsala, Sweden). In this system, binding between a molecule coupled to a biosensor chip (the "ligand") and a second molecule injected over the chip (the "analyte") results in changes in the SPR signal that are read out in real time as resonance units (RUs) (Malmqvist, 1993). dIgA was covalently coupled to a reagent-grade CM5 sensor chip (Biacore) at three different densities (412, 763, and 1426 RUs) using the primary amine coupling method described in the BIAcore manual. The first flow cell was mock coupled with buffer only for background subtraction. A 2-fold dilution concentration series (from 10.24 μM to 20 nM glycosylated D1 or from 6.4 μM to 12.5 nM nonglycosylated D1) of 180 μl of pIgR D1 (the analyte) was injected over the chip at 5 μl/min in 50 mM HEPES (pH 8.0), 150 mM NaCl, and 0.005% (v/v) P20, and the binding reactions were allowed to closely approach or to reach equilibrium. Two-minute injections of 1.5 M MgCl₂ were used to regenerate the surface of the chip between injections. The sensorgrams were processed and analyzed with the Scrubber software package (BioLogic Software, Campbell, Australia). Equilibrium dissociation constants (K_Ds) were derived by nonlinear regression analysis of plots of R_{eq} (the equilibrium binding response) versus the log of the concentration of analyte, and the resulting binding data were fit to a single-site binding model. Data collection and binding analyses were performed identically for the glycosylated and nonglycosylated forms of pIgR D1. To compare the binding of pIgR D1 to monomeric and dimeric versions of the Fc region of IgA, Fcα, Fcα-tp, and dIgA were coupled to a CM5 biosensor chip at densities of 2457 RUs, 1411 RUs, and 3153 RUs, respectively, as described above. 100 μl of 5 μM glycosylated D1,

nonglycosylated D1, or FcαRI were injected over the chip at 50 μl/min in 50 mM HEPES (pH 8.0), 150 mM NaCl, 0.005% (v/v) P20.

Crystal Growth and Data Collection
Crystals were grown by vapor diffusion in 1:1 hanging drops containing bacterially-expressed pIgR D1 (~10 mg/mL in 20 mM HEPES (pH 7.0), 150 mM NaCl), 20% (w/v) polyethylene glycol 8000 (PEG 8000), 0.2 M magnesium acetate tetrahydrate, and 0.1 M sodium cacodylate (pH 6.5) and reproduced by streak seeding. Before data collection, crystals were cryopreserved in 23% (w/v) PEG 8000, 0.2 M magnesium acetate tetrahydrate, and 0.1 M sodium cacodylate (pH 6.5) with 15% (v/v) glycerol. Heavy atom derivatives were prepared by soaking crystals in the following solutions: 1 mM di-μ-iodobis (ethylenediamine) diplatinum (II) nitrate (PIP), 40 mM trimethyl lead acetate, or 100 mM gadolinium (III) chloride. Data from a native crystal and the PIP derivative were collected at −170°C using an R-AXIS IV mounted on a Rigaku RU-200 rotating anode generator. This native data set (native I) was used for initial phase determination and model building. A higher resolution native data set (native II), which was used for refinement, and the lead and gadolinium derivative data sets were collected on beamline 8.2.2 at the Advanced Light Source (ALS, Berkeley, CA) at −170°C (Table 1).

Structure Determination and Refinement
Data were processed and scaled with DENZO and SCALEPACK (Otwinowski and Minor, 1997). The data could be indexed in either primitive monoclinic (P2_1) or C-centered orthorhombic (C222_1) space groups with unit-cell parameters a = 42.1 Å, b = 156.4 Å, c = 53.9 Å; β = 113.0° or a = 42.1 Å, b = 99.2 Å, and c = 156.4 Å, respectively. The overall scaling statistics for C222_1 were significantly worse than for P2_1 (R_{sym} = 14.3% [47.7%] versus R_{sym} = 8.5% [34.3%]) and the h0l plane did not show mm symmetry, indicating the crystals were monoclinic. After examination of systematic absences in the 0k0 reflections, the space group was assigned as P2_1. The asymmetric unit contains six molecules with a solvent content of ~40% (V_M = 2.1 Å^3/Da) as calculated from the Matthews coefficient (Matthews, 1968).

For merging the native and derivative data sets, two options for indexing had to be considered. Two identical but nonequivalent unit cells can be defined in monoclinic space groups when cosβ = −a/(2c) (Rudolph et al., 2004), a condition met by the D1 unit cell parameters. Each derivative data set was compared to two versions of the native I data set: as originally indexed, and reindexed using the transformation (h, k, l) to (h, −k, −h−l). The correct indexing of each derivative as compared to the native I data was determined by comparing R_{merge} values, which were systematically higher when the opposite indexing had been chosen for the two data sets being compared (Tucker et al., 1996).

In addition to indexing ambiguities, the D1 diffraction data exhibited evidence of pseudomerohedral twinning, a rare type of twinning that can occur in monoclinic and orthorhombic crystal systems when the unit cell parameters meet certain conditions (Rudolph et al., 2004). One such condition, as discussed above, is when cosβ = −a/(2c), in which case twinned crystals in the monoclinic system can mimic an orthorhombic space group. Since the D1 crystal parameters meet this condition, all data sets were checked for twinning. The cumulative distribution of intensities (I/<I>), as calculated with TRUNCATE (CCP4, 1994) showed a sigmoidal shape, suggesting twinning in all of the crystals. However, the second moment of intensities (<|I|^2/(<|I|>)^2) for some of the data sets was 2.0, which is the expected value for untwinned data. For the data sets with the seemingly contradictory twin test results, further examination of a related value (<|F|>^{2}/<F^2>) confirmed twinning (Brunger et al., 1998). The estimated twin fractions calculated with CNS (Brunger et al., 1998) ranged from 20.7% to 37.3% (Table 1). Similar cases of pseudomerohedral twinning in monoclinic crystal forms have been described by others (De La Fortelle and Bricogne, 1997; Larsen et al., 2002; Rudolph et al., 2004).

Heavy atom positions and initial phases were derived with the programs SOLVE (Terwilliger and Berendzen, 1999) and SHARP (De La Fortelle and Bricogne, 1997) using the native I, trimethyl lead acetate, gadolinium chloride, and PIP derivative data sets with no corrections for twinning. An initial electron density map was calculated to 2.7 Å and solvent flattened with Solomon (CCP4, 1994). The first four molecules in the asymmetric unit were located in the initial experimental map using the program MOLREP (Vagin and Teplyakov, 1997) and a "β strands-only" model of NKp44 (PDB code 1HKF) (Cantoni et al., 2003) (nonconserved side chains truncated to alanine and residues 5–9, 14–15, 25–31, 40–45, 53–55, 69–71, 80–85, 95–101, and 112 omitted). The remaining two molecules were located using the real space search program ESSENS (Kleywegt and Jones, 1997). Maps were calculated by solvent flattening and histogram matching with DM in CCP4 (CCP4, 1994). NKp44 (Cantoni et al., 2003) served as a starting point for model building with the program O (Jones and Kjeldgaard, 1997).

Refinement was performed using the CNS suite of programs (Brunger et al., 1998). The test set of reflections for calculating R_{free} was generated with the thin shell method in DATAMAN (Kleywegt and Jones, 1996) to minimize the bias from the 6-fold noncrystallographic symmetry (NCS) and twin-related reflections. Initial refinement was conducted using the 2.5 Å native I data with NCS constraints, grouped temperature (B) factors, bulk solvent and anisotropic temperature-factor corrections. In subsequent refinement using the 1.9 Å native II data set, the NCS constraints were relaxed to NCS restraints (300 kcal/mol Å^2) and individual B factors were calculated, taking into account the twin fraction of 37.3% and maintaining the same set of test reflections for calculating R_{free}. NCS restraints were limited to the main chain atoms of the β strands, excluding regions that differed in the six molecules (mostly at crystal contacts and in the loops). R_{cryst} and R_{free} improved by 5.1% and 3.4%, respectively, after inclusion of the corrections for twinning.

The final model (R_{cryst} = 18.3%, R_{free} = 24.4%) contains six D1 domains (residues 2–109) arranged as three dimers, five or six residues of the C-terminal 6×His tag in two of the six D1 domains (molecules B and A, respectively), 158 water molecules, and two Mg^{2+} ions. Each of the two Mg^{2+} ions are coordinated by three histidine residues in the 6×His tags from two molecules (His112 and His115 from molecule A with His112 from molecule F coordinate one ion and His112 and His115 from molecule B with His112 from molecule E from the adjacent asymmetric unit coordinate the other). Residue 2 in molecules B, C, and D; the CC′ loop (residues 41–45) in molecules A, B, C, and D; and the 6×His tag for molecules C, D, E, and F were disordered and are not included in the refined model, and 2.8% of the residues were modeled as alanine. The electron density is weak for residues 97–101 (with B factors averaging 49.6 Å^2, compared with an average of 32.3 Å^2 for the rest of the model). Ramachandran plot statistics were calculated using PROCHECK (Laskowski et al., 1993). Automated structural comparisons of pIgR D1 were done using the DALI server (Holm and Sander, 1993). Least-squares alignments of pIgR D1 and its closest structural homolog, the V_L and V_H domains of a mouse scFv (PDB code 1MFA), were done using O (Jones and Kjeldgaard, 1997). Sequence alignments were performed with T-Coffee (Notredame et al., 2000). Figures were generated with Molscript (Kraulis, 1991), Bobscript (Esnouf, 1997), and Raster 3D (Merrit and Murphy, 1994).

References

Al-Lazikani, B., Lesk, A.M., and Chothia, C. (1997). Standard conformations for the canonical structures of immunoglobulins. J. Mol. Biol. *273*, 927–948.

Alzari, P.M., Lascombe, M.B., and Poljak, R.J. (1988). Three-dimensional structure of antibodies. Annu. Rev. Immunol. *6*, 555–580.

Bakos, M.A., Kurosky, A., and Goldblum, R.M. (1991). Characterization of a critical binding site for human polymeric Ig on secretory component. J. Immunol. *147*, 3419–3426.

Bakos, M.A., Kurosky, A., Czerwinski, E.W., and Goldblum, R.M. (1993). A conserved binding site on the receptor for polymeric Ig is homologous to CDR1 of Ig V kappa domains. J. Immunol. *151*, 1346–1352.

Bakos, M.A., Widen, S.G., and Goldblum, R.M. (1994). Expression and purification of biologically active domain I of the human polymeric immunoglobulin receptor. Mol. Immunol. *31*, 165–168.

Bastian, A., Kratzin, H., Eckart, K., and Hilschmann, N. (1992). Intra- and interchain disulfide bridges of the human J chain in secretory immunoglobulin A. Biol. Chem. Hoppe Seyler *373*, 1255–1263.

Beale, D. (1988). Cyanogen bromide cleavage of bovine secretory component and its tryptic fragments. Int. J. Biochem. *20*, 873–879.

Brandtzaeg, P. (1973). Structure, synthesis and external transfer of mucosal immunoglobulins. Ann. Immunol. (Paris) *124*, 417–438.

Brandtzaeg, P. (1975). Human secretory immunoglobulin M. An immunochemical and immunohistochemical study. Immunology *29*, 559–570.

Brandtzaeg, P., and Prydz, H. (1984). Direct evidence for an integrated function of J chain and secretory component in epithelial transport of immunoglobulins. Nature *311*, 71–73.

Brunger, A.T., Adams, P.D., Clore, G.M., Delano, W.L., Gros, P., Grosse-Kunstleve, R.W., Jiang, J.-S., Kuszewski, J., Nilges, M., Pannu, N.S., et al. (1998). Crystallography & NMR system: a new software suite for macromolecular structure determination. Acta Crystallogr. D Biol. Crystallogr. *54*, 905–921.

Cantoni, C., Ponassi, M., Biassoni, R., Conte, R., Spallarossa, A., Moretta, A., Moretta, L., Bolognesi, M., and Bordo, D. (2003). The three-dimensional structure of the human NK cell receptor NKp44, a triggering partner in natural cytotoxicity. Structure (Camb) *11*, 725–734.

Chothia, C., and Lesk, A.M. (1987). Canonical structures for the hypervariable regions of immunoglobulins. J. Mol. Biol. *196*, 901–917.

Chothia, C., Lesk, A.M., Tramontano, A., Levitt, M., Smith-Gill, S.J., Air, G., Sheriff, S., Padlan, E.A., Davies, D., Tulip, W.R., et al. (1989). Conformations of immunoglobulin hypervariable regions. Nature *342*, 877–883.

CCP4 (Collaborative Computational Project, Number 4) (1994). The CCP4 suite: programs for protein crystallography. Acta Crystallogr. D Biol. Crystallogr. *50*, 760–763.

Coyne, R.S., Siebrecht, M., Peitsch, M.C., and Casanova, J.E. (1994). Mutational analysis of polymeric immunoglobulin receptor/ligand interactions. Evidence for the involvement of multiple complementarity determining region (CDR)-like loops in receptor domain I. J. Biol. Chem. *269*, 31620–31625.

Crottet, P., and Corthesy, B. (1998). Secretory component delays the conversion of secretory IgA into antigen-binding competent F(ab')2: a possible implication for mucosal defense. J. Immunol. *161*, 5445–5453.

Crottet, P., and Corthesy, B. (1999). Mapping the interaction between murine IgA and murine secretory component carrying epitope substitutions reveals a role of domains II and III in covalent binding to IgA. J. Biol. Chem. *274*, 31456–31462.

Dall'Acqua, W., Goldman, E.R., Eisenstein, E., and Mariuzza, R.A. (1996). A mutational analysis of the binding of two different proteins to the same antibody. Biochemistry *35*, 9667–9676.

De La Fortelle, E., and Bricogne, G. (1997). Maximum-likelihood heavy-atom parameter refinement for multiple isomorpous replacement and multiwavelength anomalous diffraction methods. Methods Enzymol. *276*, 472–494.

Deitcher, D.L., and Mostov, K.E. (1986). Alternate splicing of rabbit polymeric immunoglobulin receptor. Mol. Cell. Biol. *6*, 2712–2715.

Esnouf, R.M. (1997). An extensively modified version of MolScript that includes greatly enhanced coloring capabilities. J. Mol. Graph. Model. *15*, 132–134, 112–133.

Fallgreen-Gebauer, E., Gebauer, W., Bastian, A., Kratzin, H.D., Eiffert, H., Zimmermann, B., Karas, M., and Hilschmann, N. (1993). The covalent linkage of secretory component to IgA. Structure of sIgA. Biol. Chem. Hoppe Seyler *374*, 1023–1028.

Frutiger, S., Hughes, G.J., Hanly, W.C., Kingzette, M., and Jaton, J.C. (1986). The amino-terminal domain of rabbit secretory component is responsible for noncovalent binding to immunoglobulin A dimers. J. Biol. Chem. *261*, 16673–16681.

Garboczi, D.N., Hung, D.T., and Wiley, D.C. (1992). HLA-A2-peptide complexes: refolding and crystallization of molecules expressed in Escherichia coli and complexed with single antigenic peptides. Proc. Natl. Acad. Sci. USA *89*, 3429–3433.

Geneste, C., Iscaki, S., Mangalo, R., and Pillot, J. (1986). Both Fc α domains of human IgA are involved in in vitro interaction between secretory component and dimeric IgA. Immunol. Lett. *13*, 221–226.

Gill, S.C., and von Hippel, P.H. (1989). Calculation of protein extinction coefficients from amino acid sequence data. Anal. Biochem. *182*, 319–326.

Halpern, M.S., and Koshland, M.E. (1970). Noval subunit in secretory IgA. Nature *228*, 1276–1278.

Herr, A.B., Ballister, E.R., and Bjorkman, P.J. (2003a). Insights into IgA-mediated immune responses from the crystal structures of human FcαRI and its complex with IgA1-Fc. Nature *423*, 614–620.

Herr, A.B., White, C.L., Milburn, C., Wu, C., and Bjorkman, P.J. (2003b). Bivalent binding of IgA1 to FcαRI suggests a mechanism for cytokine activation of IgA phagocytosis. J. Mol. Biol. *327*, 645–657.

Hexham, J.M., White, K.D., Carayannopoulos, L.N., Mandecki, W., Brisette, R., Yang, Y.S., and Capra, J.D. (1999). A human immunoglobulin (Ig)A cα3 domain motif directs polymeric Ig receptor-mediated secretion. J. Exp. Med. *189*, 747–752.

Holm, L., and Sander, C. (1993). Protein structure comparison by alignment of distance matrices. J. Mol. Biol. *233*, 123–138.

Hughes, G.J., Reason, A.J., Savoy, L., Jaton, J., and Frutiger-Hughes, S. (1999). Carbohydrate moieties in human secretory component. Biochim. Biophys. Acta *1434*, 86–93.

Jones, T.A., and Kjeldgaard, M. (1997). Electron density map interpretation. Methods Enzymol. *277*, 173–208.

Kelley, R.F., and O'Connell, M.P. (1993). Thermodynamic analysis of an antibody functional epitope. Biochemistry *32*, 6828–6835.

Kleywegt, G.J., and Jones, T.A. (1996). xdlMAPMAN and xdlDATAMAN—programs for reformatting, analysis and manipulation of biomacromolecular electron-density maps and reflection data sets. Acta Crystallogr. D Biol. Crystallogr. *52*, 826–828.

Kleywegt, G.J., and Jones, T.A. (1997). Template convolution to enhance or detect structural features in macromolecular electron-density maps. Acta Crystallogr. D Biol. Crystallogr. *53*, 179–185.

Kraulis, P.J. (1991). MOLSCRIPT: a program to produce both detailed and schematic plots of protein structures. J. Appl. Crystallogr. *24*, 946–950.

Larsen, N.A., Heine, A., de Prada, P., Redwan el, R., Yeates, T.O., Landry, D.W., and Wilson, I.A. (2002). Structure determination of a cocaine hydrolytic antibody from a pseudomerohedrally twinned crystal. Acta Crystallogr. D Biol. Crystallogr. *58*, 2055–2059.

Laskowski, R.A., MacArthur, M.W., Moss, D.S., and Thornton, J.M. (1993). PROCHECK: a program to check the stereochemical quality of protein structures. J. Appl. Crystallogr. *26*, 283–291.

Lebron, J.A., and Bjorkman, P.J. (1999). The transferrin receptor binding site on HFE, the class I MHC-related protein mutated in hereditary hemochromatosis. J. Mol. Biol. *289*, 1109–1118.

Malmqvist, M. (1993). Biospecific interaction analysis using biosensor technology. Nature *361*, 186–187.

Matsumoto, N., Asano, M., Ogura, Y., Takenouchi-Ohkubo, N., Chihaya, H., Chung-Hsing, W., Ishikawa, K., Zhu, L., and Moro, I. (2003). Release of non-glycosylated polymeric immunoglobulin receptor protein. Scand. J. Immunol. 58, 471–476.

Matthews, B.W. (1968). Solvent content of protein crystals. J. Mol. Biol. 33, 491–497.

McDonald, K.J., Cameron, A.J., Allen, J.M., and Jardine, A.G. (2002). Expression of Fc α/μ receptor by human mesangial cells: a candidate receptor for immune complex deposition in IgA nephropathy. Biochem. Biophys. Res. Commun. 290, 438–442.

Merrit, E.A., and Murphy, M.E.P. (1994). Raster3d, a program for photorealistic molecular graphics. Acta Crystallogr. D Biol. Crystallogr. 50, 869–873.

Mestecky, J., Zikan, J., and Butler, W.T. (1971). Immunoglobulin M and secretory immunoglobulin A: presence of a common polypeptide chain different from light chains. Science 171, 1163–1165.

Mostov, K.E., Kraehenbuhl, J.P., and Blobel, G. (1980). Receptormediated transcellular transport of immunoglobulin: synthesis of secretory component as multiple and larger transmembrane forms. Proc. Natl. Acad. Sci. USA 77, 7257–7261.

Mostov, K.E., Friedlander, M., and Blobel, G. (1984). The receptor for transepithelial transport of IgA and IgM contains multiple immunoglobulin-like domains. Nature 308, 37–43.

Norderhaug, I.N., Johansen, F.E., Krajci, P., and Brandtzaeg, P. (1999a). Domain deletions in the human polymeric Ig receptor disclose differences between its dimeric IgA and pentameric IgM interaction. Eur. J. Immunol. 29, 3401–3409.

Norderhaug, I.N., Johansen, F.E., Schjerven, H., and Brandtzaeg, P. (1999b). Regulation of the formation and external transport of secretory immunoglobulins. Crit. Rev. Immunol. 19, 481–508.

Notredame, C., Higgins, D.G., and Heringa, J. (2000). T-Coffee: A novel method for fast and accurate multiple sequence alignment. J. Mol. Biol. 302, 205–217.

Otwinowski, Z., and Minor, W. (1997). Processing of X-ray diffraction data collected in oscillation mode. Methods Enzymol. 276, 307–326.

Piskurich, J.F., Blanchard, M.H., Youngman, K.R., France, J.A., and Kaetzel, C.S. (1995). Molecular cloning of the mouse polymeric Ig receptor. Functional regions of the molecule are conserved among five mammalian species. J. Immunol. 154, 1735–1747.

Radl, J., Klein, F., van den Berg, P., de Bruyn, A.M., and Hijmans, W. (1971). Binding of secretory piece to polymeric IgA and IgM paraproteins in vitro. Immunology 20, 843–852.

Roe, M., Norderhaug, I.N., Brandtzaeg, P., and Johansen, F.E. (1999). Fine specificity of ligand-binding domain 1 in the polymeric Ig receptor: importance of the CDR2-containing region for IgM interaction. J. Immunol. 162, 6046–6052.

Rudolph, M.G., Wingren, C., Crowley, M.P., Chien, Y.H., and Wilson, I.A. (2004). Combined pseudo-merohedral twinning, non-crystallographic symmetry and pseudo-translation in a monoclinic crystal form of the gammadelta T-cell ligand T10. Acta Crystallogr. D Biol. Crystallogr. 60, 656–664.

Shibuya, A., Sakamoto, N., Shimizu, Y., Shibuya, K., Osawa, M., Hiroyama, T., Eyre, H.J., Sutherland, G.R., Endo, Y., Fujita, T., et al. (2000). Fc α/μ receptor mediates endocytosis of IgM-coated microbes. Nat. Immunol. 1, 441–446.

Socken, D.J., and Underdown, B.J. (1978). Comparison of human, bovine and rabbit secretory component-immunoglobulin interactions. Immunochemistry 15, 499–506.

Song, W., Vaerman, J.P., and Mostov, K.E. (1995). Dimeric and tetrameric IgA are transcytosed equally by the polymeric Ig receptor. J. Immunol. 155, 715–721.

Terwilliger, T.C., and Berendzen, J. (1999). Automated MAD and MIR structure solution. Acta Crystallogr. D Biol. Crystallogr. 55, 849–861.

Tsumoto, K., Ogasahara, K., Ueda, Y., Watanabe, K., Yutani, K., and Kumagai, I. (1995). Role of Tyr residues in the contact region of antilysozyme monoclonal antibody HyHEL10 for antigen binding. J. Biol. Chem. 270, 18551–18557.

Tucker, A.D., Rowsell, S., Melton, R.G., and Pauptit, R.A. (1996). A new crystal form of carboxypeptidase G2 from Pseudomonas sp. strain RS-16 which is more amenable to structure determination. Acta Crystallogr. D Biol. Crystallogr. 52, 890–892.

Underdown, B.J., Switzer, I., and Jackson, G.D. (1992). Rat secretory component binds poorly to rodent IgM. J. Immunol. 149, 487–491.

Vaerman, J.P., Langendries, A., and Vander Maelen, C. (1995). Homogenous IgA monomers, dimers, trimers and tetramers from the same IgA myeloma serum. Immunol. Invest. 24, 631–641.

Vaerman, J.P., Langendries, A., Giffroy, D., Brandtzaeg, P., and Kobayashi, K. (1998a). Lack of SC/pIgR-mediated epithelial transport of a human polymeric IgA devoid of J chain: in vitro and in vivo studies. Immunology 95, 90–96.

Vaerman, J.P., Langendries, A.E., Giffroy, D.A., Kaetzel, C.S., Fiani, C.M., Moro, I., Brandtzaeg, P., and Kobayashi, K. (1998b). Antibody against the human J chain inhibits polymeric Ig receptor-mediated biliary and epithelial transport of human polymeric IgA. Eur. J. Immunol. 28, 171–182.

Vagin, A., and Teplyakov, A. (1997). MOLREP: an automated program for molecular replacement. J. Appl. Crystallogr. 30, 1022–1025.

van Egmond, M., van Garderen, E., van Spriel, A.B., Damen, C.A., van Amersfoort, E.S., van Zandbergen, G., van Hattum, J., Kuiper, J., and van de Winkel, J.G. (2000). FαRI-positive liver Kupffer cells: reappraisal of the function of immunoglobulin A in immunity. Nat. Med. 6, 680–685.

Vaughn, D.E., Milburn, C.M., Penny, D.M., Martin, W.L., Johnson, J.L., and Bjorkman, P.J. (1997). Identification of critical IgG binding epitopes on the neonatal Fc receptor. J. Mol. Biol. 274, 597–607.

Vidarsson, G., van Der Pol, W.L., van Den Elsen, J.M., Vile, H., Jansen, M., Duijs, J., Morton, H.C., Boel, E., Daha, M.R., Corthesy, B., and van De Winkel, J.G. (2001). Activity of human IgG and IgA subclasses in immune defense against Neisseria meningitidis serogroup B. J. Immunol. 166, 6250–6256.

Wells, J.A., and de Vos, A.M. (1996). Hematopoietic receptor complexes. Annu. Rev. Biochem. 65, 609–634.

White, K.D., and Capra, J.D. (2002). Targeting mucosal sites by polymeric immunoglobulin receptor-directed peptides. J. Exp. Med. 196, 551–555.

Wieland, W.H., Orzaez, D., Lammers, A., Parmentier, H.K., Verstegen, M.W., and Schots, A. (2004). A functional polymeric immunoglobulin receptor in chicken (Gallus gallus) indicates ancient role of secretory IgA in mucosal immunity. Biochem. J. 380, 669–676.

Williams, A.F., and Barclay, A.N. (1988). The immunoglobulin superfamily—domains for cell surface recognition. Annu. Rev. Immunol. 6, 381–405.

Zdanov, A., Li, Y., Bundle, D.R., Deng, S.J., MacKenzie, C.R., Narang, S.A., Young, N.M., and Cygler, M. (1994). Structure of a singlechain antibody variable domain (Fv) fragment complexed with a carbohydrate antigen at 1.7-A resolution. Proc. Natl. Acad. Sci. USA 91, 6423–6427.

Accession Numbers

Atomic coordinates have been deposited in the Protein Data Bank with accession code 1XED.